Physica B 406 (2011) 2254–2260

Contents lists available at ScienceDirect

Physica B

journal homepage: www.elsevier.com/locate/physb

First principles study of structural, vibrational and electronic properties of graphene-like MX_2 (M=Mo, Nb, W, Ta; X=S, Se, Te) monolayers

Yi Ding [a,*], Yanli Wang [b,*], Jun Ni [c], Lin Shi [d], Siqi Shi [b], Weihua Tang [b]

[a] Department of Physics, Hangzhou Normal University, Hangzhou, Zhejiang 310036, People's Republic of China
[b] Department of Physics, Center for Optoelectronics Materials and Devices, Zhejiang Sci-Tech University, Xiasha College Park, Hangzhou, Zhejiang 310018, People's Republic of China
[c] Department of Physics, Key Laboratory of Atomic and Molecular Nanoscience (Ministry of Education), Tsinghua University, Beijing 100084, People's Republic of China
[d] Suzhou Institute of Nano-Tech and Nano-Bionics, Chinese Academy of Sciences, Suzhou 215125, People's Republic of China

ARTICLE INFO

Article history:
Received 25 January 2011
Received in revised form
17 March 2011
Accepted 18 March 2011
Available online 23 March 2011

Keywords:
Graphene-like structure
Electronic structure
First principles calculation

ABSTRACT

Using first principles calculations, we investigate the structural, vibrational and electronic structures of the monolayer graphene-like transition-metal dichalcogenide (MX_2) sheets. We find the lattice parameters and stabilities of the MX_2 sheets are mainly determined by the chalcogen atoms, while the electronic properties depend on the metal atoms. The NbS_2 and TaS_2 sheets have comparable energetic stabilities to the synthesized MoS_2 and WS_2 ones. The molybdenum and tungsten dichalcogenide (MoX_2 and WX_2) sheets have similar lattice parameters, vibrational modes, and electronic structures. These analogies also exist between the niobium and tantalum dichalcogenide (NbX_2 and TaX_2) sheets. However, the NbX_2 and TaX_2 sheets are metals, while the MoX_2 and WX_2 ones are semiconductors with direct-band gaps. When the Nb and Ta atoms are doped into the MoS_2 and WS_2 sheets, a semiconductor-to-metal transition occurs. Comparing to the bulk compounds, these monolayer sheets have similar structural parameters and properties, but their vibrational and electronic properties are varied and have special characteristics. Our results suggest that the graphene-like MX_2 sheets have potential applications in nano-electronics and nano-devices.

1. Introduction

Since the discovery of graphene [1,2], two-dimensional nanostructures have attracted lots of interests in nano-science and condensed matter physics [3–8]. Graphene is a monolayer carbon hexagonal sheet, which has a unique massless Dirac-like electronic excitation [3]. The two-dimensional graphene sheet is a semimetal, while for the graphene with finite width, it becomes a semiconductor or a half-metal depending on the edge shapes [4,5]. In the experiments, graphene sheets are initially obtained by micro-mechanical cleavage technique, using which the mono- and few-layer sheets are pulled from the layered graphite material [2]. Recently, several chemical methods, such as epitaxial growth on SiC surfaces, chemical vapor deposition on metal surfaces, reduction of graphite oxide, have been reported for the high-yield production of graphene [7–9]. Besides carbon-based nanostructures, other inorganic nanomaterials, especially whose structures are analogous to graphene, have also been synthesized and investigated [10]. For example, the two-dimensional BN sheet has been successfully synthesized by the micro-mechanical cleavage technique and chemical-solution-derived method [11]. Through high-resolution transmission electron microscopy, it has been observed that B and N atoms occupy one sublattice of the hexagonal sheet, respectively [12]. Different from graphene, due to the inequivalence of the two sublattices, the two-dimensional BN sheet is a wide band-gap semiconductor [13].

Binary metal-dichalcogenides also have similar layered structures as graphite. By chemical bath deposition method and the mechanochemical route, the molybdenum disulfide (MoS_2) films have been obtained in the experiments [14]. Besides, the two-dimensional MoS_2 sheet has been reported by micro-mechanical cleavage as early as the time of graphene [2]. Recently, the monolayer MoS_2 sheet has been successfully synthesized by chemical methods in the experiment [15]. Previous theoretical studies show that bulk MoS_2 is an indirect-band-gap semiconductor [16,17], while the two-dimensional MoS_2 sheet is a direct-band-gap semiconductor [18]. The MoS_2 sheet could be rolled up into MoS_2 nanotubes, which are all semiconductors regardless of the chirality [19]. While for the MoS_2 sheets of finite width, the corresponding nanoribbons become ferromagnetic metals [20]. Similar to the MoS_2 sheet, the graphene-like WS_2 nanostructure has also been synthesized [15]. The corresponding WS_2 nanotubes are also semiconductors [21]. From Landolt–Börnstein database [22], we find that the

* Corresponding authors. Tel./fax: +86 057128865286.
E-mail addresses: dingyi2001@tsinghua.org.cn (Y. Ding), wangyanli-04@tsinghua.org.cn (Y. Wang).

0921-4526/$ - see front matter © 2011 Elsevier B.V. All rights reserved.
doi:10.1016/j.physb.2011.03.044

$MoSe_2$, $MoTe_2$, NbS_2, $NbSe_2$, WS_2, WSe_2, TaS_2, and $TaSe_2$ materials have the same layered structural type as that of MoS_2. However, among those materials, previous studies have only been performed on the two-dimensional sheets of the MoS_2, $NbSe_2$, and WS_2 systems [15,18]. Thus, it is promising to perform a systemic study on those graphene-like sheets, which is helpful for the fabrications and applications of those nanomaterials.

In this paper, we investigate the structural, vibrational and electronic properties of the two-dimensional MX_2 (M=Mo, Nb, W, Ta; X=S, Se, Te) sheets by first principles calculations. The lattice parameters, charge transfers, cohesive energies, Raman active and infrared active vibrational modes, and the band gaps of the MX_2 sheets are obtained and compared to the bulk ones in detail. We also discuss the metal doping effects and predict a semiconductor-to-metal transition in the MoS_2 and WS_2 sheets.

2. Methods

The first principle calculations are performed by VASP with a plane-wave set and projector augmented wave pseudopotentials [23]. Two types of exchange and correlation (XC) functionals, the Ceperly–Alder functional form of the local density approximation (LDA) and the Perdew–Burke–Ernzerhof (PBE) functional form of the generalized gradient approximation (GGA) are adopted in the calculations. The plane-wave cutoff energy is set to be 400 eV. The supercells are used to simulate the isolated sheets and in order to avoid interlayer interactions, the distance between sheets is set to larger than 12 Å. The lattice constants and the atom coordinates are optimized until the convergence of the force on each atom is less than 0.01 eV/Å. The Monkhorst–Pack scheme is used to sample the Brillouin zone. The structures are fully relaxed with a mesh of $12\times12\times1$, and the mesh of k space is increased to $15\times15\times1$ and $24\times24\times1$ in the static and density of state (DOS) calculations, respectively.

3. Results

3.1. Structural properties

The crystal structure of the monolayer MoS_2 sheet is shown in Fig. 1(a). Similar to BN, SiC, ZnO and other heterogeneous graphene-like sheets, Mo atoms occupy one sublattice of the hexagonal sheet and S atoms occupy the other. However, due to the chemical ratio of Mo:S=1:2, the Mo sublattice layer is sandwiched between two nearby S sublattice layers. We obtain the thickness of the MoS_2 sheet is 3.13 Å (3.12 Å) and the length of the Mo–S bond is 2.42 Å(2.39 Å) by the PBE (LDA) calculations. These calculated values agree well with the previous calculations by Li [20] and Ramakrishna Matte [15]. The optimized lattice constant of the MoS_2 sheet is 3.19 Å (3.13 Å) with PBE (LDA), which is almost the same as the bulk value of 3.15 Å [20].

All the lattice parameters of the MX_2 sheets are listed in Table 1. It can be seen that the MoX_2 and WX_2 sheets, the NbX_2 and TaX_2 sheets have quite similar lattice parameters. For the same chalcogen, the difference of metals affects the lattice parameters slightly. For example, the in-sheet lattice constants of NbS_2 and TaS_2 sheets are only 0.15 Å longer than those of the MoS_2 and WS_2 ones. Four disulfide sheet, MoS_2, WS_2, NbS_2, and TaS_2 sheets, have a general thickness of 3.1 Å. However, different chalcogen atoms change the lattice parameters significantly. The diselenide and ditelluride sheets increase the thickness to 3.3 and 3.6 Å, respectively. Due to the increase of the chalcogen atomic radius, both the bond lengths d_{M-X} and the in-sheet lattice constants also increase in the sequence of $MS_2<MSe_2<MTe_2$ for the same metal atoms.

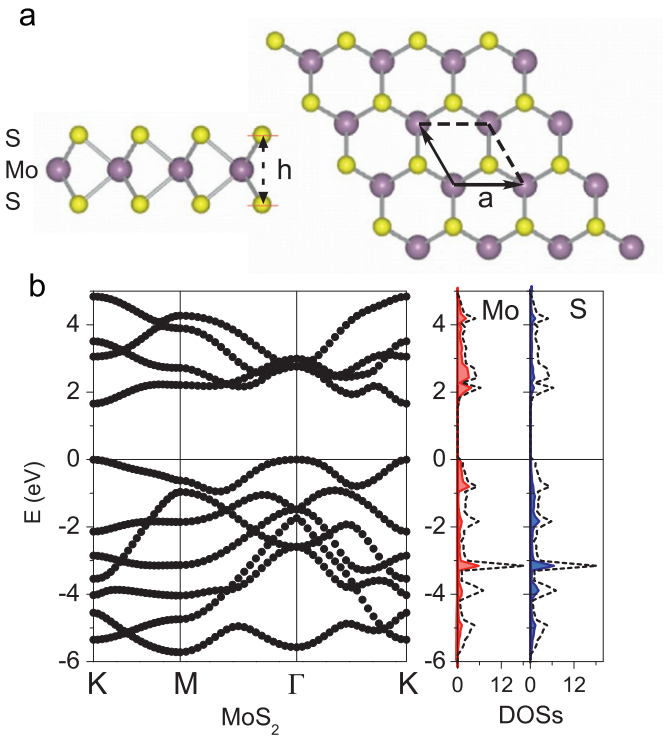

Fig. 1. (a) The side and top view of the graphene-like MoS_2 sheet. (b) The band structure, total and partial DOSs for the Mo d and S p orbitals. The dot lines represent the total DOSs of the MoS_2 sheet. The Fermi level is indicated as the line at $E=0.0$ eV.

The difference of chalcogens affects not only the lattice parameters, but also the cohesive energies. In our calculations, the cohesive energies are defined as $E_c(MX_2)=E_{MX_2}-E_{M\ atom}-2\times E_{X\ atom}$. Here, E_{MX_2} is the total energy of the MX_2 sheet, $E_{M\ atom}$ and $E_{X\ atom}$ are the energies of the corresponding metal and chalcogen isolated atoms. When the cohesive energies are more negative, the MX_2 sheets are more favorable. For the MoS_2 sheet, our PBE calculations show the formation energy is -5.07 eV/atom, which is in accordance with the GGA result of -5.20 eV/atom and the pseudo-atomic numerical orbitals result of -5.00 eV/atom [20]. While the LDA calculations predict a larger value of -6.25 eV/atom. This phenomenon is common for the first principles calculations, since the LDA XC functional normally gets short lattices and high energies, while the GGA one has the contrary trends [24,25]. From Table 1, it can be seen that $E_c(MS_2)<E_c(MSe_2)<E_c(MTe_2)$. Using the Bader analysis [26], we obtain the charge transfers from the metal to the chalcogen atoms. As shown in Table 1, in the MoS_2 sheet, the Mo atom loses 0.90 e and each S atom gains 0.45 e. While in the $MoSe_2$ and $MoTe_2$ sheets, the charge transfers of Mo atoms decrease to 0.76 and 0.24 e, respectively. Due to the small charge transfers and elongated lattice constants, the cohesive energies of the $MoSe_2$ and $MoTe_2$ sheets decrease to -4.53 and -3.97 eV/atom, respectively. Since the W, Nb, and Ta atoms transfer more electrons to the chalcogen atoms than the Mo atoms, their corresponding sheets will have higher cohesive energies than the MoX_2 systems. We also calculate the formation energies of the MX_2 sheets as $E_{form}=E_{MX_2}-E_{M\ bulk}-2\times E_{X\ dimer}$. Here, $E_{M\ bulk}$ and $E_{X\ dimer}$ represent the atomic energies in their stable elemental structures. For the metals, the stable structure is a body-centered cubic (bcc) bulk with the Im-3m space group, while for the chalcogens, the stable structure is a molecular dimer. As shown in Table 1, all the MX_2 sheets have negative formation energies, which means the composing processes from the elemental forms are exothermic reactions and those MX_2 sheets are stable. The E_{form} of MoS_2 and

Table 1
The lattice constants a, bond lengths d_{M-X}, sheet thicknesses h, cohesive energies E_c, formation energies E_{form}, charge transfers of metals ΔQ, vibrational frequencies at the Γ point, and electronic properties of the MX_2 (M=Mo, Nb, W, Ta; X=S, Se, Te) sheets. The PBE and LDA represent the XC functionals used in the calculations.

		a (Å)	d_{M-X} (Å)	h (Å)	E_c (eV/atom)	E_{form} (eV/atom)	ΔQ (e)	E'' (cm^{-1})	E' (cm^{-1})	A_1' (cm^{-1})	A_2'' (cm^{-1})	
MoS_2	PBE	3.19	2.42	3.13	−5.07	−1.42	0.90	276	374	396	457	Semiconductor
	LDA	3.13	2.39	3.12	−6.25	−1.71	0.86	290	392	411	475	Semiconductor
$MoSe_2$	PBE	3.33	2.55	3.35	−4.53	−1.21	0.76	160	277	233	343	Semiconductor
	LDA	3.25	2.51	3.32	−5.73	−1.50	0.84	168	291	243	359	Semiconductor
$MoTe_2$	PBE	3.56	2.74	3.62	−3.97	−0.86	0.24	114	230	167	285	Semiconductor
	LDA	3.47	2.69	3.60	−5.13	−1.14	0.24	120	241	174	300	Semiconductor
WS_2	PBE	3.19	2.42	3.14	−5.71	−1.37	1.00	287	344	409	426	Semiconductor
	LDA	3.13	2.39	3.13	−6.90	−1.65	0.98	300	360	423	441	Semiconductor
WSe_2	PBE	3.32	2.55	3.36	−5.10	−1.09	0.60	166	238	241	298	Semiconductor
	LDA	3.25	2.51	3.34	−6.31	−1.38	0.68	174	249	250	311	Semiconductor
WTe_2	PBE	3.56	2.74	3.63	−4.46	−0.66	0.19	118	192	172	239	Semiconductor
	LDA	3.47	2.70	3.61	−5.63	−0.95	0.24	124	200	180	250	Semiconductor
NbS_2	PBE	3.36	2.49	3.14	−5.44	−1.56	1.06	215	295	372	373	Metal
	LDA	3.29	2.46	3.12	−6.45	−1.81	1.04	232	315	383	389	Metal
$NbSe_2$	PBE	3.48	2.62	3.37	−4.92	−1.37	0.90	123	230	221	284	Metal
	LDA	3.41	2.58	3.34	−5.96	−1.63	0.92	131	242	228	296	Metal
$NbTe_2$	PBE	3.70	2.82	3.69	−4.34	−1.01	0.36	91	199	154	241	Metal
	LDA	3.59	2.78	3.69	−5.35	−1.26	0.36	95	199	153	260	Metal
TaS_2	PBE	3.34	2.48	3.13	−5.92	−1.60	1.12	230	282	355	387	Metal
	LDA	3.28	2.47	3.10	−6.87	−1.85	1.10	242	298	368	401	Metal
$TaSe_2$	PBE	3.48	2.62	3.36	−5.34	−1.35	0.92	130	198	230	251	Metal
	LDA	3.40	2.57	3.32	−6.31	−1.60	0.88	135	209	238	261	Metal
$TaTe_2$	PBE	3.71	2.82	3.66	−4.67	−0.91	0.34	94	166	164	201	Metal
	LDA	3.61	2.77	3.64	−5.62	−1.15	0.34	97	173	169	212	Metal

WS_2 sheets are −1.42 and −1.37 (−1.71 and −1.65) eV/atom by the PBE (LDA) calculations. Comparing the E_c and E_{form} of the MX_2 sheets in Table 1, we find that the NbS_2 and TaS_2 sheets have higher cohesive and formation energies than the synthesized MoS_2 and WS_2 ones. It is possible to produce these sheets from their bulk structures by similar chemical methods for the MoS_2 and WS_2 materials [15].

3.2. Vibrational properties

For the low-dimensional nanostructures, Raman spectra is one important characterization tool in the experiments [27]. Recently, two groups have measured the Raman shift of the MoS_2 sheets [15,28]. Here, we use the finite displacements methods to investigate the zone-centered vibrational properties of the MX_2 sheets. Since the MX_2 monolayer has the symmetry of D_{3h} point group, besides three acoustic modes, the six optical modes at the Γ point can be classified as follows: $\Gamma_{opt} = 2E''(R)+2E'(I+R)+A_1'(R)+A_2''(I)$. The R and I represent the vibrational modes having Raman and infrared activities, respectively. Fig. 2 shows the atomic displacements for each vibrational mode. The E'' and E' modes represent the in-sheet movements of atoms, which are doubly degenerate due to the equivalence of x and y-axes. For the E'' mode, only the chalcogen atoms move oppositely. The frequency of this mode is less than 300 cm^{-1}, which is beyond the range of experimental measurements [15,28]. For the E' mode, two chalcogen atoms move in the same direction and the metal atom moves oppositely. The calculated frequency is 374 cm^{-1} with PBE and 392 cm^{-1} with LDA. Lee et al. measure the monolayer MoS_2 sample and obtain the E' mode is in the range of 381−385 cm^{-1} [28]. Ramakrishna Matte et al. report a frequency of 379.7 cm^{-1} for the MoS_2 film [15]. Comparing to these experimental values, the PBE calculation is underestimated, while the LDA one is overestimated. The A_1' and A_2'' modes are non-degenerate. Both modes represent the out-sheet movements of atoms as shown in Fig. 2(a). The A_1' mode is the Raman active vibration, whose frequency is 396 (411) cm^{-1} for the PBE (LDA) calculations. In the experiments, Lee et al. obtain the A_1' mode is in the range of 401−407 cm^{-1} [28], and Ramakrishna Matte et al. get a value of 404.7 cm^{-1} [15]. Our calculated results agree well with these experimental values within 2% deviations. The A_2'' mode is an infrared active frequency of about 460 cm^{-1}, which needs further experimental verifications.

For other MX_2 sheets, the corresponding vibrational frequencies are listed in Table 1. Since the E' and A_1' modes are usually measured in the experiments [15,28], we focus on these two modes for different MX_2 sheets. The E' and A_1' modes of the WS_2 sheet are 344 (360) and 409 (423) cm^{-1} by the PBE (LDA) calculations, which also agree well with the experimental results [15]. Since the movements of the chalcogen atoms contribute to the displacements mainly, the vibrational frequencies of the E' and A_1' modes are determined by the chalcogen atoms. Taking the MoX_2 sheets as an example, the E' mode of the $MoSe_2$ sheet decreases by about 100 cm^{-1} compared to the MoS_2 sheet. The out-sheet vibrational frequency of the $MoSe_2$ sheet also decreases fast as shown in Fig. 2. The A_1' mode reduces to 233 cm^{-1}, which becomes less than the E' mode. When the chalcogen atoms are the Te element, the $MoTe_2$ sheet has the E' and A_1' frequencies down to 230 and 167cm^{-1}, respectively. For other WX_2, NbX_2, TaX_2 systems, we also obtain that the frequencies of E' and A_1' modes follow the order of $MS_2 > MSe_2 > MTe_2$.

3.3. Electronic properties

Although the difference of chalcogen atoms affects the structural and vibrational properties, it has little influence on the electronic properties. Figs. 1(c) and (d) show the electronic structure of the MoS_2 sheet. The MoS_2 sheet is a semiconductor with a direct-band gap at the K point. The PBE (LDA) gap value

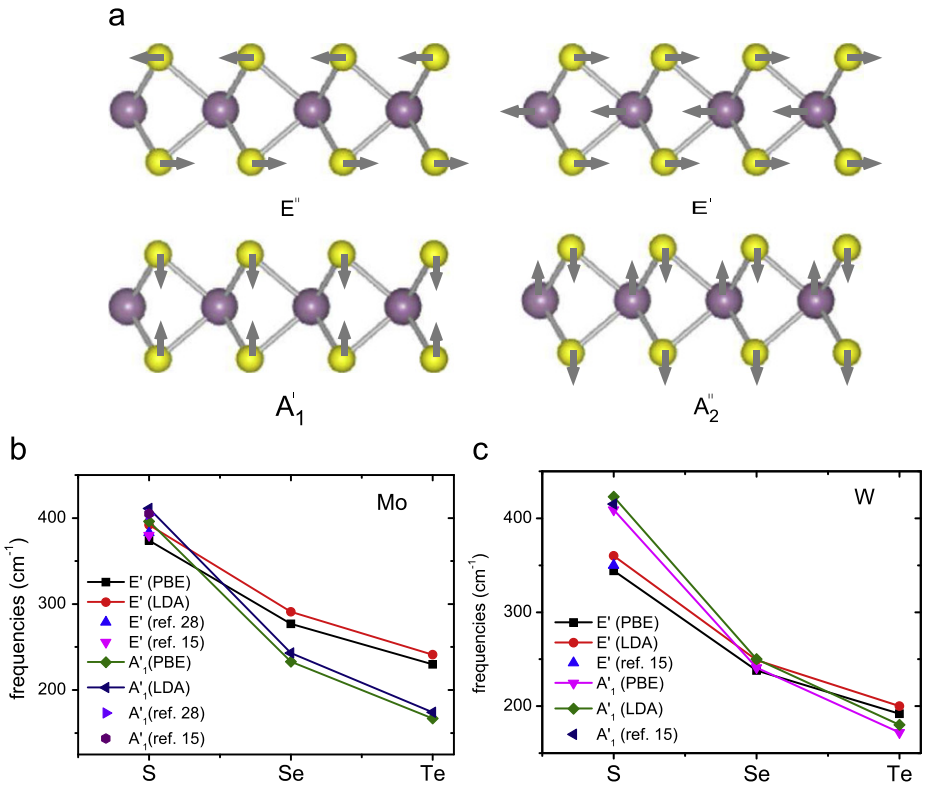

Fig. 2. (a) The vibrational modes of MX_2 sheets. Arrows in the figure represent directions of the atomic displacements for each mode. The vibrational frequencies of E' and A_1' modes for (b) MoX_2 and (c) WX_2 sheets.

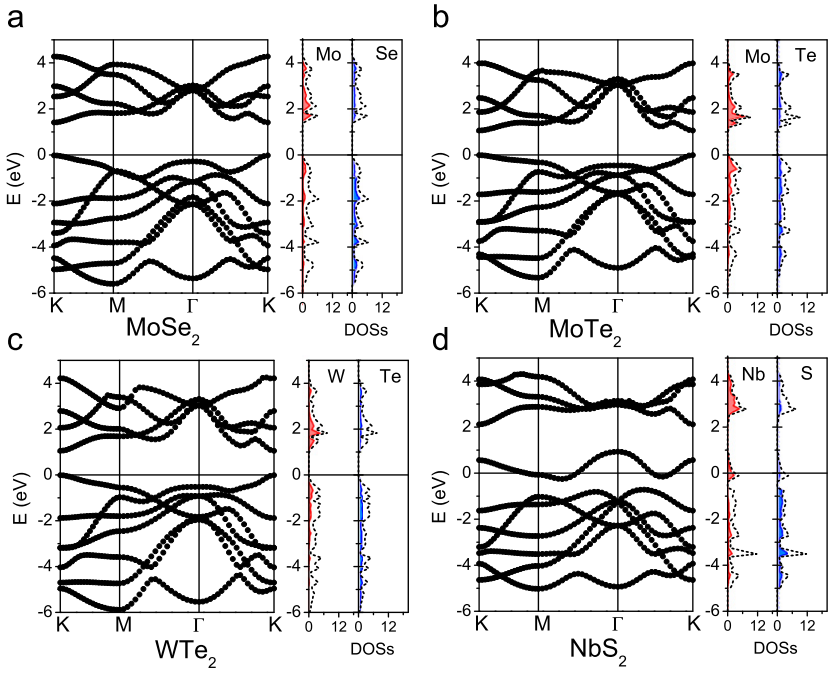

Fig. 3. The band structures, total and partial DOSs of the (a) $MoSe_2$, (b) $MoTe_2$, (c) WTe_2, and (d) NbS_2 sheets.

is 1.67 (1.86) eV, which agrees well with the latest MoS_2 photoluminescence experiment [29] and previous theoretical studies [18,20]. Similar to the MoS_2 sheet, both the $MoSe_2$ and $MoTe_2$ ones are also direct-band-gap semiconductors as shown in Figs. 3(a) and (b). Fig. 3(c) displays the typical band structure of the WTe_2 sheet. For the three WX_2 sheets, we find they have analogous semiconducting properties. However, both the NbX_2 and TaX_2 sheets become metals. As shown in Fig. 3(d), the NbS_2 sheet exhibits metallic behavior with one band crossing the Fermi level. The partial DOS analysis indicates this band is mainly attributed to the d orbitals of Nb atoms. Since the Nb (Ta) atom is one d electron less than the Mo (W) atom, the top d-character valence bands are not fully occupied and the metallicity appears in the NbX_2 (TaX_2) sheets. This result is consistent with the

experimental observation that the TaS_2 films present robust metallic behaviors [30]. Thus, these metallic NbX_2 and TaX_2 sheets would be one type of conducting materials for nano-devices.

For the semiconducting MoX_2 and WX_2 sheets, the calculated PBE and LDA band gaps are listed in Table 2. It is well-known that the traditional DFT calculations perform well for the properties of the ground state, but generally underestimate the band gaps of materials [24]. In order to predict accurate band gaps, extra calculations are carried out by two ways. One way is utilizing the Heyd–Scuseria–Ernzerhof (HSE) hybrid XC functional. Comparing with the PBE results, the HSE calculations increase the band gaps by about 0.5 eV. The band gaps of the MoS_2 and WS_2 sheets are up to 2.25 and 2.32 eV, respectively. The other way is doing the GW correction. The GW correction greatly increases the band gaps. As shown in Table 2, the MoX_2 and WX_2 sheets have the GW gaps ranging from 1.8 to 3 eV. However, no matter whether the traditional XC functional, hybrid XC functional, or GW correction is used, the band gaps of the MoX_2 and WX_2 sheets follow the same order of disulfide > diselenide > ditelluride. Considering that those direct-gaps are around 2–3 eV, the semiconducting MoX_2 and WX_2 sheets can be used as solar energy materials, luminescent materials, and so on.

Table 2
The calculated band gaps at the *K*-point of the semiconducting MoX_2 and WX_2 sheets within different XC functionals of PBE, LDA, HSE, and GW correction.

	PBE (eV)	LDA (eV)	HSE (eV)	GW (eV)
MoS_2	1.67	1.86	2.25	2.66
$MoSe_2$	1.44	1.63	1.99	2.31
$MoTe_2$	1.07	1.23	1.59	1.77
WS_2	1.81	1.94	2.32	2.91
WSe_2	1.55	1.74	2.10	2.51
WTe_2	1.06	1.14	1.55	1.79

Next, we consider the metal-doped effects on the MX_2 sheets. Since the MoS_2 and WS_2 sheets have been successfully fabricated [15] and the Nb atom can substitute Mo atom in the MoS_2 bulk material [31], we investigate four situations as the Nb-, W-doped MoS_2 sheet and the Ta-, Mo-doped WS_2 sheet. A 3×3 supercell is used, in which the distance between the doped atoms is larger than 9.5 Å. For the Nb-doped MoS_2 sheet, the formation energy is denoted as $E_{form} = E_{Nb-MoS_2} - E_{pure\ MoS_2} - E_{Nb\ atom} + E_{Mo\ atom}$. Here, E_{Nb-MoS_2} and $E_{pure\ MoS_2}$ correspond to the total energies of Nb-doped and pure MoS_2 sheets, respectively. The $E_{form}(Nb-MoS_2)$ is calculated to be -0.84 eV/unit. Similarly, we obtain $E_{form}(W-MoS_2) = -1.93$ eV/unit, $E_{form}(Ta-WS_2) = -0.38$ eV/unit, and $E_{form}(Mo-WS_2) = 1.90$ eV/unit. The negative formation energies indicate the corresponding substitutional reactions could happen.

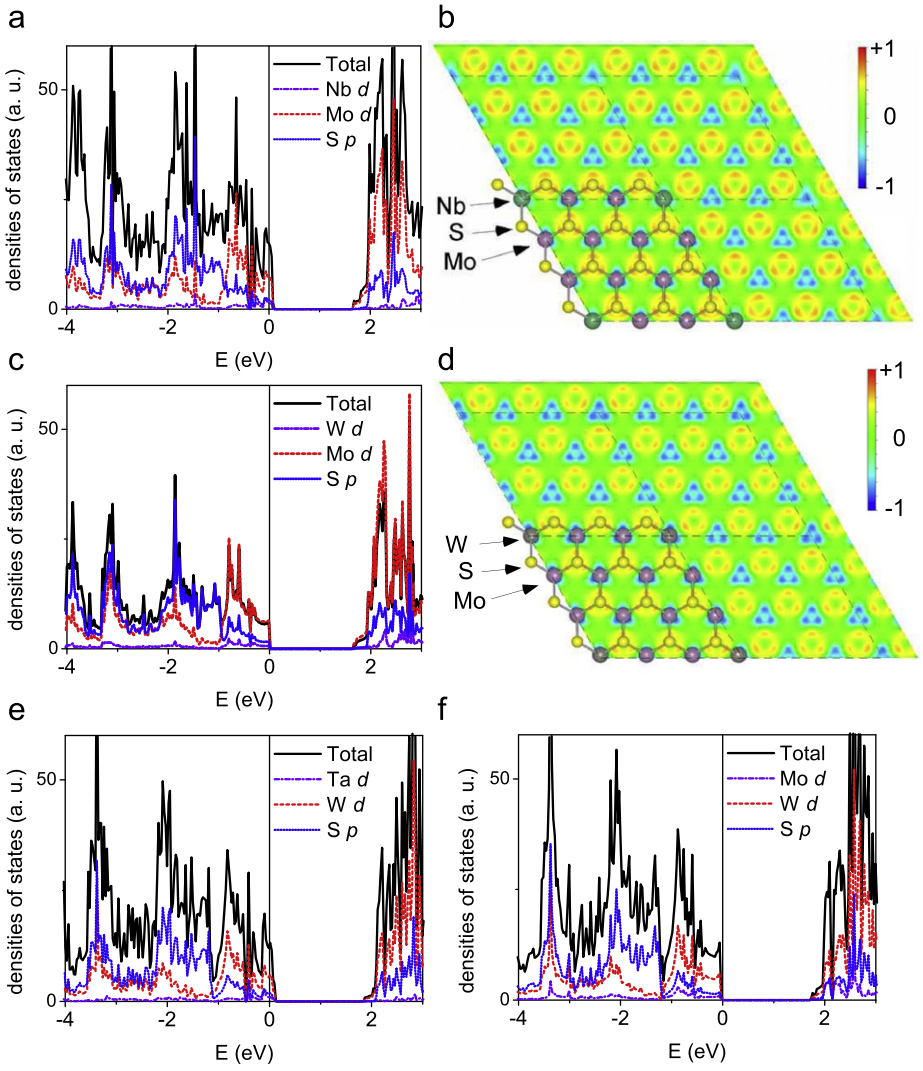

Fig. 4. (a and c) The total and partial DOSs of the Nb-doped and W-doped MoS_2 sheets. (b and d) The corresponding charge differences of the doping systems. (e and f) The total and partial DOSs of the Ta-doped and Mo-doped WS_2 sheets.

Thus, the Nb-doped MoS_2, W-doped MoS_2 and Ta-doped WS_2 sheets are possible to be formed in the experiments. Fig. 4 shows the electronic properties of those doping systems. The Nb-doped MoS_2 sheet becomes a metal. From the charge difference in Fig. 4(b), we can see the Nb atoms lose more electrons than the Mo atoms. Considering the Nb atom is one d-electron less than the Mo atom, the Nb atoms act as holes doped in the MoS_2 sheet. It causes the downshift of the Fermi level and induces a semiconductor-to-metal transition in the MoS_2 sheet. While the W atoms behave quite similarly to the Mo atoms, little is changed after W doping in the MoS_2 sheet. The W-doped MoS_2 sheet is a semiconductor with a PBE band gap of 1.65 eV, which is almost identical to that of the pure MoS_2 sheet. In the WS_2 sheet, like the Nb-doped MoS_2 system, the Ta doping induces a semiconductor-to-metal transition shown in Fig. 4(e). While for the Mo doping, Fig. 4(f) displays the Mo-doped WS_2 sheet is still a semiconductor with a PBE band gap of 1.75 eV.

Table 3

The lattice constants a and c (Å), bond lengths d_{M-X} (Å), sheet thicknesses h (Å), cohesive energies E_c (eV/atom), formation energies E_{form} (eV/atom), charge transfers of metals ΔQ (e), and vibrational frequencies at the Γ point (cm^{-1}) of the bulk 2 H-like disulfide compounds. The PBE and LDA represent the XC functionals used in the calculations.

		a	d_{M-X}	h	c	E_c	E_{form}	ΔQ	E'	A_1'
MoS_2	PBE	3.19	2.42	3.13	14.22	−5.07	−1.42	1.06	374	396
	LDA	3.13	2.39	3.12	12.09	−6.29	−1.75	1.03	389	411
WS_2	PBE	3.19	2.42	3.15	13.64	−5.71	−1.37	0.88	344	405
	LDA	3.13	2.39	3.13	12.13	−6.93	−1.69	1.00	357	423
NbS_2	PBE	3.36	2.49	3.14	13.38	−5.44	−1.57	1.31	280	372
	LDA	3.29	2.46	3.12	11.88	−6.50	−1.86	1.20	307	388
TaS_2	PBE	3.34	2.48	3.13	13.38	−5.92	−1.60	1.14	280	388
	LDA	3.27	2.45	3.11	11.98	−6.92	−1.89	1.13	293	400

4. Discussions

Finally, we compare the structures and properties of the monolayer sheets to the bulk 2 H-like structures [16,20,31]. Table 3 shows the calculated results of bulk disulfide compounds. Since the PBE XC functional is hard to describe the van der Waals interactions between the layers, which give much longer lattice constants along the c-axis than the experimental values [22], we just compare the LDA results and find the similarities and differences of monolayer sheets to the bulks as following: (1) The sheets and bulks have similar structural properties. From Tables 1 and 3, it can been seen that the lattice parameters within the layered structure such as in-sheet constant a, bond length d_{M-X}, sheet thickness h are almost the same for the sheets and bulks. However, the metals transfer less charges to the S atoms in the sheets than in the bulks, which induces a little weaker cohesive energies for the monolayers. For the MoS_2 sheet, its E_c is 0.04 eV/atom lower than the bulk one. Similarly, the WS_2, NbS_2, and TaS_2 sheets also have a little smaller cohesive energies than the bulks. These energy differences between the bulks and monolayers are about 0.04–0.05 eV/atom. Comparing with the normal room temperature (0.025 eV), it indicates that producing the disulfide sheets from their bulk structures is energetically feasible. (2) The vibrational properties of sheets are different from the bulks. The E' frequencies of the bulks are all smaller than those in the sheets. While for the A_1' mode, the frequencies are nearly the same for the MoS_2 and WS_2 sheets and bulks, but for the NbS_2 and TaS_2 compounds, the frequencies of the monolayers are smaller than those of the bulks. In the experiments, those E' and A_1' modes have been used to distinguish the components and thickness of MoS_2 layers [28,32], and Lee et al. have reported that the E' mode softens, while the A_1' mode stiffens with the increase of the MoS_2 sample thickness [28]. Our calculated results are in accordance with this phenomenon, and predict the E' and A_1' modes for the NbS_2 and TaS_2 compounds will have stronger thickness dependence. (3) The electronic properties of sheets are also varied. Fig. 5 depicts the

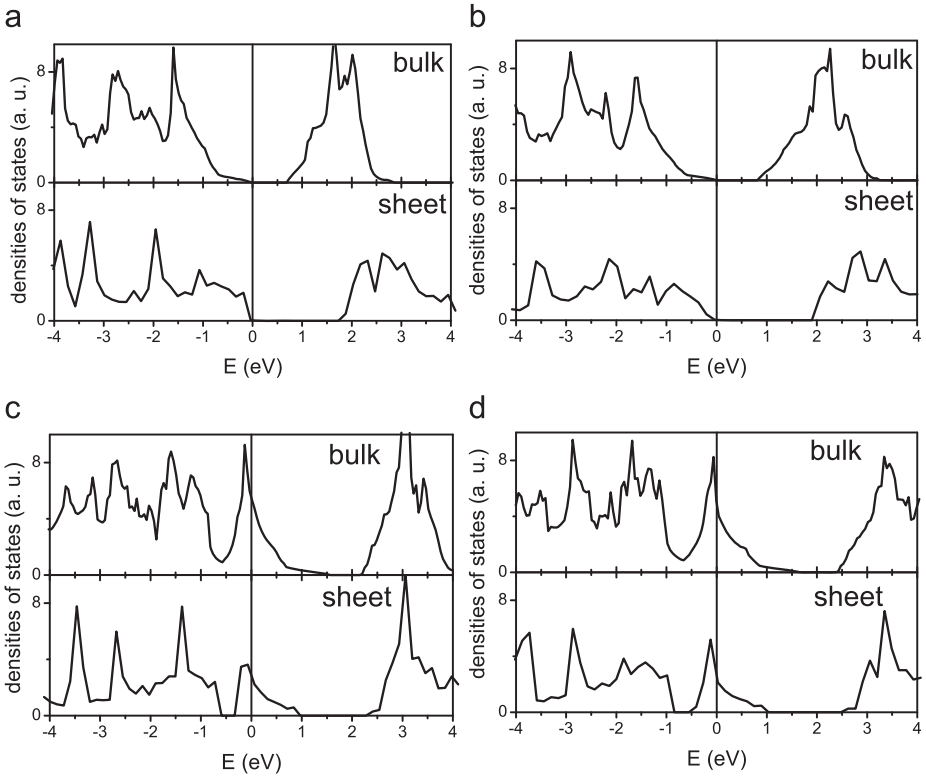

Fig. 5. The DOSs of bulk and monolayer MS_2 (M=Mo, W, Nb, Ta) compounds. (a) MoS_2, (b) WS_2, (c) NbS_2 and (d) TaS_2.

electronic structures of bulk and monolayer disulfide compounds. The MoS_2 and WS_2 sheets have large direct-band gaps of 1.86 and 1.94 eV, respectively, while their corresponding bulks possess smaller indirect-band gaps of 0.74 and 0.86 eV. For the NbS_2 and TaS_2 compounds, although the sheets maintain the metallic behavior of the bulks, the DOSs of the sheets at the Fermi level are about half of those in the bulks as shown in Figs. 5(c) and (d).

5. Conclusions

In summary, we have investigated the structural, vibrational, and electronic properties of the graphene-like MX_2 monolayers by first principles calculations. We find that:

(1) The NbS_2 and TaS_2 sheets are even more stable than the synthesized MoS_2 and WS_2 ones, which suggests it is possible to produce these sheets from their bulk structures by similar chemical methods for the MoS_2 and WS_2 materials.
(2) The MoX_2 and WX_2 sheets have similar lattice parameters, vibrational modes, as well as electronic structures. Analogous relationships also exist between the NbX_2 and TaX_2 sheets. However, the MoX_2 and WX_2 sheets are semiconductors, while the NbX_2 and TaX_2 ones are metals.
(3) The hybrid HSE functional and GW calculations show the semiconducting sheets have the band gaps of about 1.5−3 eV, which follow the order of $MS_2 > MSe_2 > MTe_2$. When doping the Nb and Ta atoms into the sheets, a semiconductor-to-metal transition occurs in the MoS_2 and WS_2 systems.
(4) Comparing to the bulk compounds, these monolayer sheets have similar structural parameters and properties, but their vibrational and electronic properties are varied. The semiconducting sheets have larger band gaps than the bulk compounds, and the metallic sheets have much smaller DOSs at the Fermi level than the bulk ones.

Our studies demonstrate that transition-metal dichalcogenide sheets, the inorganic analogs of graphene, have rich electronic structures for potential applications in nano-electronics, molecular sensing, and optical devices.

Acknowledgments

Authors acknowledge the supports from HZNU (Grant No. 2011QDL016), ZSTU (Grant No. 0913847-Y), and NSFC (Grant No. 10974107). Y. Ding would like to thank Dr. Baoxing Li, Dr. Chao Cao, HZNU College of Science, and its HPC Center for helps.

References

[1] K.S. Novoselov, A.K. Geim, S.V. Morozov, D. Jiang, Y. Zhang, S.V. Dubonos, I.V. Grigorieva, A.A. Firsov, Science 306 (2004) 666.
[2] K.S. Novoselov, D. Jiang, F. Schedin, T.J. Booth, V.V. Khotkevich, S.V. Morozov, A.K. Geim, Proc. Natl. Acad. Sci. USA 102 (2005) 10451.
[3] A.H. Castro Neto, F. Guinea, N.M.R. Peres, K.S. Novoselov, A.K. Geim, Rev. Mod. Phys. 81 (2009) 109;
A.K. Geim, Science 324 (2009) 1530.
[4] Y.-W. Son, M.L. Cohen, S.G. Louie, Nature (London) (2006) 347.
[5] M. Ezawa, Eur. Phys. J. B 66 (2008) 245;
W.H. Liao, B.H. Zhou, H.Y. Wang, G.H. Zhou, Eur. Phys. J. B 76 (2010) 463.
[6] L. Hu, X. Hu, X. Wu, C. Du, Y. Dai, J. Deng, Physica B 405 (2010) 3337;
R. Thapa, D. Sen, M.K. Mitra, K.K. Chattopadhyay, Physica B 406 (2011) 368.
[7] C.N.R. Rao, A.K. Sood, K.S. Subrahmanyam, A. Govindaraj, Angew. Chem. Int. Ed. 48 (2009) 7752.
[8] S. Park, R.S. Ruoff, Nat. Nanotechnol. 4 (2009) 217.
[9] M. Ye, Y.T. Cui, Y. Nishimura, Y. Yamada, S. Qiao, A. Kimura, M. Nakatake, H. Namatame, M. Taniguchi, Eur. Phys. J. B 75 (2010) 31.
[10] R. Tenne, Angew. Chem. Int. Ed. 42 (2003) 5124;
R. Tenne, Nat. Nanotechnol. 1 (2006) 103.
[11] D. Pacilé, J.C. Meyer, C.Ö. Girit, A. Zettl, Appl. Phys. Lett. 92 (2008) 133107;
W.-Q. Han, L. Wu, Y. Zhu, K. Watanabe, T. Taniguchi, Appl. Phys. Lett. 93 (2008) 223103.
[12] C. Jin, F. Lin, K. Suenaga, S. Iijima, Phys. Rev. Lett. 102 (2009) 195505.
[13] M. Topsakal, E. Aktürk, S. Ciraci, Phys. Rev. B 79 (2009) 115442;
Y. Wang, Phys. Status Solidi - Rapid Res. Lett. 4 (2010) 34;
S. Azevedo, J.R. Kaschny, C.M.C. de Castilho, F. de Brito Mota, Eur. Phys. J. B 67 (2009) 507.
[14] K.M. Garadkar, A.A. Patil, P.P. Hankare, P.A. Chate, D.J. Sathe, S.D. Delekar, J. Alloys Compd. 487 (2009) 786;
Z. Wu, D. Wang, A. Sun, J. Alloys Compd. 492 (2010) L5.
[15] H.S.S. Ramakrishna Matte, A. Gomathi, A.K. Manna, D.J. Late, R. Datta, S.K. Pati, C.N.R. Rao, Angew. Chem. Int. Ed. 49 (2010) 4059.
[16] R.A. Bromley, Phys. Lett. A 33 (1970) 242.
[17] L. Wei, C. Jun-fang, H. Qinyu, W. Teng, Physica B 405 (2010) 2498.
[18] S. Lebégue, O. Eriksson, Phys. Rev. B 79 (2009) 115409.
[19] G. Seifert, H. Terrones, M. Terrones, G. Jungnickel, T. Frauenheim, Phys. Rev. Lett. 85 (2000) 146;
I. Milosević, B. Nikolić, E. Dobardzić, M. Damnjanović, I. Popov, G. Seifert, Phys. Rev. B 76 (2007) 233414.
[20] Y. Li, Z. Zhou, S. Zhang, Z. Chen, J. Am. Chem. Soc. 130 (2008) 16739;
A.R. Botello-Méndez, F. López-Urías, M. Terrones, H. Terrones, Nanotechnology 20 (2009) 325703.
[21] G. Seifert, H. Terrones, M. Terrones, G. Jungnickel, T. Frauenheim, Solid State Commun. 114 (2000) 245;
G. Seifert, H. Terrones, M. Terrones, T. Frauenheim, Solid State Commun. 115 (2000) 635.
[22] Landolt-Börnstein database, Springer Publishing Company 〈http://www.springermaterials.com〉, 2010.
[23] G. Kresse, J. Furthmuller, Comput. Mater. Sci. 6 (1996) 15;
G. Kresse, J. Furthmuller, Phys. Rev. B 54 (1996) 11169.
[24] J. Hafner, J. Comput. Chem. 29 (2008) 2044.
[25] P. Haas, F. Tran, P. Blaha, S. Pedroza, J.R. da Silva, M. Odashima, K. Capelle, Phys. Rev. B 81 (2010) 125136.
[26] W. Tang, E. Sanville, G. Henkelman, J. Phys. Condens. Matter 21 (2009) 084204.
[27] M.S. Dresselhaus, G. Dresselhaus, R. Saito, A. Jorio, Phys. Rep. 409 (2005) 47.
[28] C. Lee, H. Yan, L.E. Brus, T.F. Heinz, J. Hone, S. Ryu, ACS Nano 4 (2010) 2695.
[29] A. Splendiani, L. Sun, Y. Zhang, T. Li, J. Kim, C.-Y. Chim, G. Galli, F. Wang, Nano Lett. 10 (2010) 1271.
[30] A. Ayari, E. Cobas, O. Ogundadegbe, M.S. Fuhrerb, J. Appl. Phys. 101 (2007) 014507.
[31] V.V. Ivanovskaya, A. Zobelli, A. Gloter, N. Brun, V. Serin, C. Colliex, Phys. Rev. B 78 (2008) 134104.
[32] D.O. Dumcenco, K.Y. Chen, Y.P. Wang, Y.S. Huang, K.K. Tiong, J. Alloys Compd. 506 (2010) 940.